

pubs.acs.org/JACS Communication

# Connected Peptide Modules Enable Controlled Co-Existence of Self-Assembled Fibers Inside Liquid Condensates

Ankit Jain,\*<sup>,</sup> Salma Kassem, Rachel S. Fisher, Biran Wang, Tai-De Li, Tong Wang, Ye He, Shana Elbaum-Garfinkle,\* and Rein V. Ulijn\*



Cite This: J. Am. Chem. Soc. 2022, 144, 15002-15007



**ACCESS** I

III Metrics & More

Article Recommendations

Supporting Information

ABSTRACT: Supramolecular self-assembly of fibrous components and liquid—liquid phase separation are at the extremes of the order-to-disorder spectrum. They collectively play key roles in cellular organization. It is still a major challenge to design systems where both highly ordered nanostructures and liquid—liquid phase-separated domains can coexist. We present a three-component assembly approach that generates fibrous domains that exclusively form inside globally disordered, liquid condensates. This is achieved by creating amphiphilic peptides that combine the features of fibrillar assembly (the amyloid domain LVFFA) and complex coacervation (oligo-arginine and adenosine triphosphate (ATP)) in one peptide, namely, LVFFAR<sub>9</sub>. When this hybrid peptide is mixed in different ratios with R<sub>9</sub> and ATP, we find that conditions can be created where fibrous assembly is exclusively observed inside liquid coacervates. Through fluorescence and atomic force microscopy characterization, we investigate the dynamic evolution of ordered and disordered features over time. It was observed that the fibers nucleate and mature inside the droplets and that these fiber-containing liquid droplets can also undergo fusion, showing that the droplets remain liquid-like. Our work thus generates opportunities for the design of ordered structures within the confined environment of biomolecular condensates, which may be useful to create supramolecular materials in defined compartments and as model systems that can enhance understanding of ordering principles in biology.

B iomolecular condensates represent a growing area of research, due to their recognized importance in subcellular organization of biological structures, chemical origins of life, the design of biomimetic materials, and the development of new tools for synthetic biology. <sup>1-6</sup> In most cases, biological condensates are multicomponent systems that bring various components together, thereby enhancing component proximity and flux, which results in regulation of reaction specificity. <sup>7-9</sup> A plethora of examples in which local environments generated in condensates lead to spatially controlled properties have been reported, including enhanced enzyme activity, selective uptake of reaction components, localized changes in dielectric constants, overall control of binding events, and even noise buffering. <sup>10-16</sup>

Recent evidence suggests that most biological condensates lie in between homogeneous liquids and heterogeneous aggregates with a range of mixed phases observed. S,17,18 Over time, condensates can transition between states; for example, many protein systems associated with pathological aggregation in neurodegenerative diseases, such as FUS [RNA binding protein FUsed in Sarcoma], can mature through a liquid-to-solid transition. Similarly, short peptides that mimic amyloid aggregation have been shown to undergo a two-stage process involving liquid—liquid phase separation (LLPS) followed by fiber nucleation and growth.

Globally disordered or liquid systems that contain local ordered domains have been traditionally difficult to design, as they mostly, over time, lead to gels or aggregates representing lower free-energy states.<sup>21</sup> To our knowledge, the existence of ordered fiber domains inside liquid condensates has only been

achieved by specialized proteins. <sup>22–24</sup> Therefore, development of a minimalistic multicomponent system that promotes local order in globally disordered systems such as coacervates is warranted. <sup>25,26</sup> Besides gaining understanding of navigating order and disorder in biological design spaces, one can foresee applications in supramolecular materials, including those relevant to catalysis and selective sequestration in compartments. <sup>27</sup>

In this work, we show controlled generation of supramolecular fiber domains in liquid condensates by combining well-known minimalistic peptide domains. Key to our design is an amphiphilic peptide that combines the features of fibrillar assembly (through the amyloid domain LVFFA) and complex coacervation (oligo-arginine/ATP)<sup>8</sup> in one peptide, namely, LVFFAR<sub>9</sub>. Combining LVFFAR<sub>9</sub> in varying ratios with R<sub>9</sub> as positively charged components and ATP as a negatively charged counterpart forms the basis of three component condensates (Figure 1a). The LVFFA motif was selected due to its self-assembly into a  $\beta$ -sheet structural component in the  $A\beta$  system<sup>28,29</sup> that has been extensively explored in minimalistic supramolecular peptide assemblies.<sup>30–32</sup> We envisaged that R<sub>9</sub>-ATP interactions would give rise to a tricomponent coassembly

Received: June 7, 2022 Published: August 10, 2022





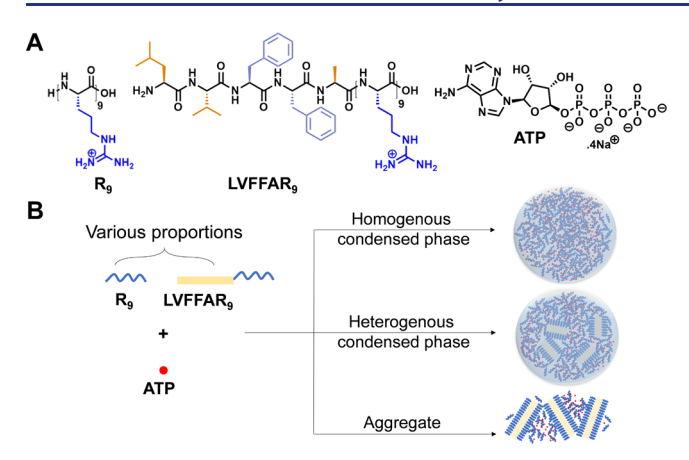


**Figure 1.** Design of self-assembled fibers inside liquid peptide condensates and prospective morphological outcomes dictated by composition. (a) Molecular structures of the two positively charged oligopeptides used to form coacervates with ATP. (b) Schematic detailing the use of various proportions of positively charged species in conjunction with ATP to form coacervates and the resulting morphologies.

 $(R_9 + LVFFAR_9 + ATP)$  where local proximity of the LVFFA motif would lead to amyloid formation exclusively inside the droplets, with the  $R_9$  moiety stabilizing the amyloid-coacervate interface. Furthermore, since the mole percentage of LVFFAR\_9 can be controlled, this is expected to lead to control over aggregated domain formation in a globally disordered liquid of  $R_9$  and ATP (Figure 1b).

We combined  $R_0$  and LVFFAR $_0$  in various proportions such that the overall net positive charge concentration in solution is always 10 mM (based on nine charge equivalents per R<sub>o</sub> molecule). This is countered by 10 mM negatively charged counterions provided by ATP (four charge equivalents). The mixture of R<sub>9</sub>/LVFFAR<sub>9</sub> was added to the solution containing ATP, which resulted in coacervation as evidenced by instantaneous generation of an inhomogeneous solution. The pH of the mixture was maintained at 8.0 buffered by 10 mM Tris·HCl containing 15 mM KCl, 0.5 mM MgCl<sub>2</sub>, and 0.2% (w/ v) NaN<sub>3</sub>. To understand the effect of the different components and phase separation on LVFFAR, fibril formation, we measured the critical aggregation concentration (CAC) of LVFFAR<sub>9</sub> in the presence of R<sub>9</sub> and ATP alone (no coacervates formed) and compared this with the CAC in Ro-ATP coacervates (Supporting Information Figure S1). We found that, while  $R_9$  alone has no significant impact on the CAC, the presence of ATP in equivalent charge concentration reduced the CAC by more than twofold (from 1.37 to 0.56 mM), due to minimization of charge repulsion. The confinement of the LVFFA motif within liquid droplets further reduced its CAC by more than 4 times to 0.12 mM (12% in respect to  $\mathbf{R}_{9}$  in the three component droplets). Atomic force microscopy (AFM) showed that the morphology of LVFFAR<sub>9</sub> assemblies changes significantly in the presence of ATP and Ro-ATP coacervates forming aggregates and short fibers, entangled fibers, and bundled densely packed fibers, respectively (Supporting Information Figure S2).

To visualize the formation of peptide fibers inside coacervates by confocal microscopy, we used Alexa-fluor 488 functionalized peptide LVFFAR<sub>9</sub>-[C]-AF488 (f-LVFFAR<sub>9</sub>) and Alexa-fluor 647 functionalized ATP (f-ATP) that can be readily observed through separate channels (Each dye concentration = 2.5  $\mu$ M).

Coacervates consisting of various percentages of LVFFAR<sub>9</sub> were formed, below and above the CAC (0%-100%) in  $\mathbb{R}_{9}$  with ATP (Figure 2a). The samples were imaged through sandwiched, surface-functionalized (with N-(triethoxysilylpropyl)-O-poly-(ethylene oxide) urethane, details in the Methods section of the Supporting Information) coverslips using a confocal microscope. Surface functionalization was done to reduce coalescence of droplets on glass surface. We observed heterogeneous condensed phases at 20% LVFFAR<sub>9</sub> as a stabilized phase (up to one week) between homogeneous coacervates (at 0-5% LVFFAR<sub>9</sub>) and aggregates (at >50% LVFFAR<sub>9</sub>) (Figure 2a, Supporting Information Figure S3). The colocalization of ATP and amyloids suggests interactions across the multicomponent system stabilizing the interface of the fibrillar structures and the condensate. An orthogonal sectioning of these droplets showed well-dispersed fibers inside, pointing to a coexistence of fibers inside droplets (Supporting Information Figure S4, Supporting Information Videos S1 & S2). Cryotransmission electron microscopy (Cryo-TEM) also confirmed the presence of fibrillar structures, 10-20 nm in width, within the droplets with 20% LVFFAR<sub>9</sub> (Supporting Information Figure S5) indicating that the fibers observed by confocal microscopy are composed of bundles of nanofibers. These were obtained from samples where the coacervates had been dissolved by increasing the salt concentration in the system (addition of 3 M NaCl) after 10 h of maturation. This is because the size of the droplets (18  $\mu$ m<sup>3</sup> on average) is too thick for electron penetration and imaging by TEM and cryo-EM. The micrographs however clearly show the confinement of fibrillar networks inside the perimeter of spherical shapes corresponding to the perimeter of the dissolved droplets.

We further characterized droplets with various percentages of LVFFAR<sub>9</sub> with fluorescence recovery after photobleaching (FRAP) (Dye: 0.5% f-LVFFAR<sub>9</sub>, Figure 2b). While 0% LVFFAR<sub>9</sub> containing condensates showed nearly complete recovery, confirming their liquid-like nature, the extent of recovery decreased with increasing percentages of the LVFFAR<sub>9</sub>. The progressive decrease in mobile fraction with increasing amyloid percentage is consistent with an increase in the solid fraction of the system. Snapshots of FRAP on condensates containing 20% LVFFAR, over time also demonstrate the lack of recovery in the amyloid parts of the droplet (Figure 2c, Supporting Information Figure S6, Supporting Information Video S3). We further characterized the heterogeneous condensates with 20% LVFFAR9 using traditional  $\beta$ -sheet staining dyes, Thioflavin-T, and Congo Red (Supporting Information Figure S7). We observed staining and fluorescence enhancement in samples containing the amyloid forming domains, further confirming that the structures are indeed  $\beta$ -sheets formed due to LVFFA motif aggregation. Further evidence showing that these fibers are confined in a liquid medium comes during the investigation of fiber dynamics. We show that fiber-containing droplets merge to form bigger droplets, with aspect ratio going from 2.1 (separate droplets) to 1.0 (completely merged droplets) in 41 s (droplets are pre-aged for 2 h, Figure 2d, Supporting Information Video S4). Furthermore, to demonstrate the coexistence of ordered and disordered phases we treated the droplets with a 3 M NaCl solution, which we expected to dissolve the liquid phase (Supporting Information Video S5 & S6, Supporting Information Figure S8). On the one hand, droplets with 0% LVFFAR9 dissolved completely as the ionic strength of the resultant solution increased. On the other hand, a residual

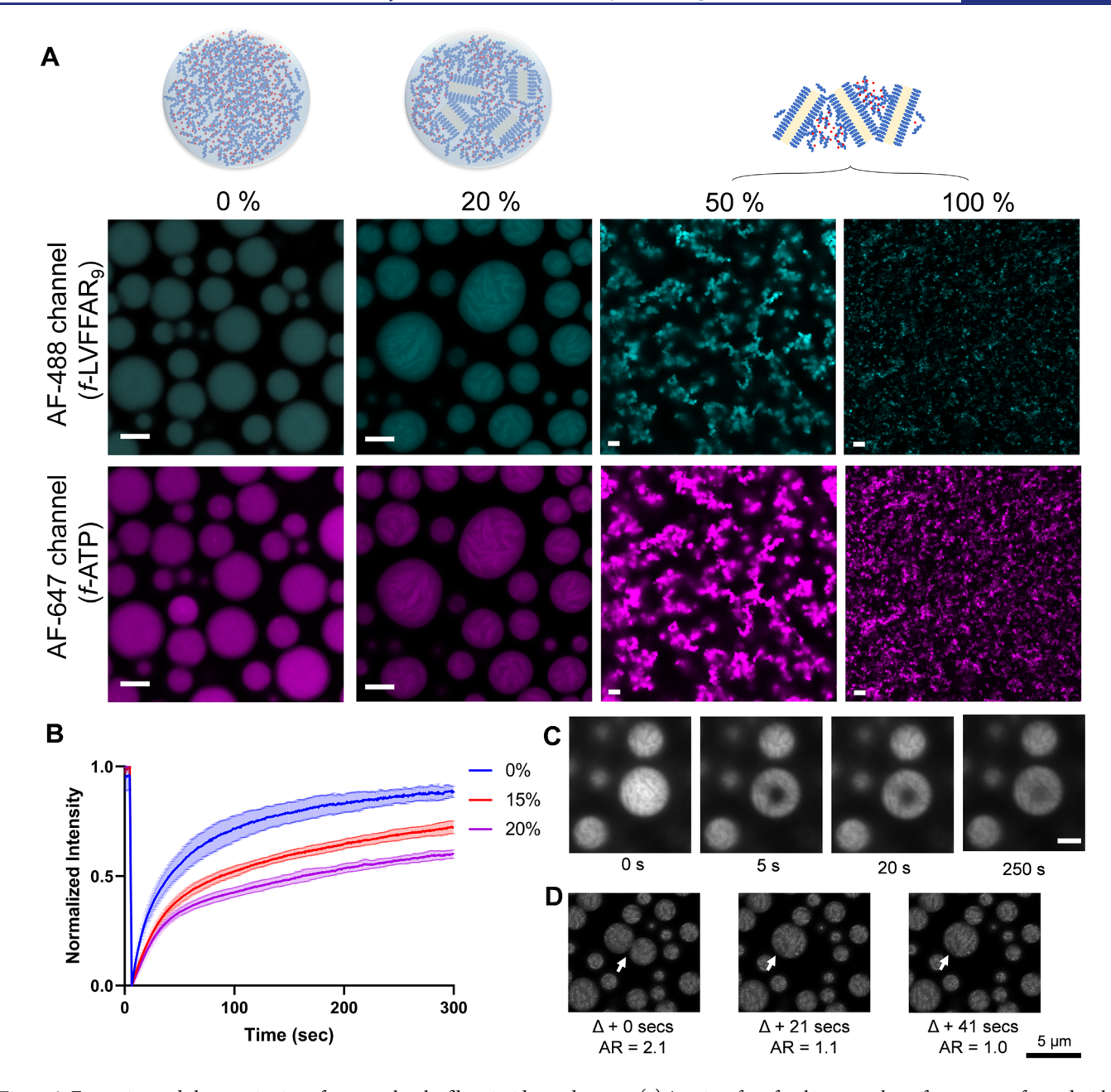


Figure 2. Formation and characterization of supramolecular fibers inside condensates. (a) A series of confocal images taken of coacervates formed with various percentages of LVFFAR<sub>9</sub>. Scale bar = 5 μm. Dyes = 0.5% *f*-LVFFAR<sub>9</sub> and 0.5% *f*-ATP excited at 488 and 647 nm, respectively. (b) FRAP traces of coacervates formed with various percentages of LVFFAR<sub>9</sub>. Dye = 0.5% *f*-LVFFAR<sub>9</sub>. (c) Confocal images corresponding to FRAP in coacervates formed with 20% LVFFAR<sub>9</sub> over time. Scale bar =  $5 \mu$ m. (d) Confocal images showing droplet merger over time (indicated by a white arrow) formed with 20% LVFFAR<sub>9</sub>. Figure also indicates the aspect ratio (AR) of the droplets over time.  $\Delta = 2.68$  h, dye = 0.5% *f*-LVFFAR<sub>9</sub> (Incubation time for all samples discussed here is 2 h).

amyloidal network (albeit modified due to hydrophobic collapse) can be seen to sustain the salt concentration, while the liquid  $R_9$  + ATP component disappears in tricomponent condensates formed with 20% LVFFAR $_9$ .

To analyze the nature of fibrilization, we studied the condensates formed with 20% LVFFAR<sub>9</sub> over time (up to 6 h) (Figure 3). Starting from the fluorescence profile of coacervates, we could see generation of amyloid fibers in individual liquid droplets. These fibers can be seen elongating in intermediate maturation times. The nucleation starts within 1.5 h, leading to maturation by 6 h (Figure 3a,b, Supporting Information Figure S9). The amount of LVFFAR<sub>9</sub> in the supernatant and condensate phases were quantified by liquid

chromatography-mass spectrometry (LC-MS) (Supporting Information Figure S10). In the droplets, the concentration of the amyloid peptide increased over time, reaching the CAC threshold (0.12 mM) between 1 and 2 h, while the concentration in the supernatant decreased and remained considerably lower (more than 5 times) than the fibril forming concentration range (above 0.56 mM in absence of droplets). The growth of fibers had no significant effect on the partitioning of R<sub>9</sub> and ATP in the condensates (Supporting Information Figure S11). A FRAP analysis over time showed that the mobile component of the droplets retains its liquid-like recovery (Dye: 0.5% f-LVFFAR<sub>9</sub>, Figure 3c, Supporting Information Videos S7

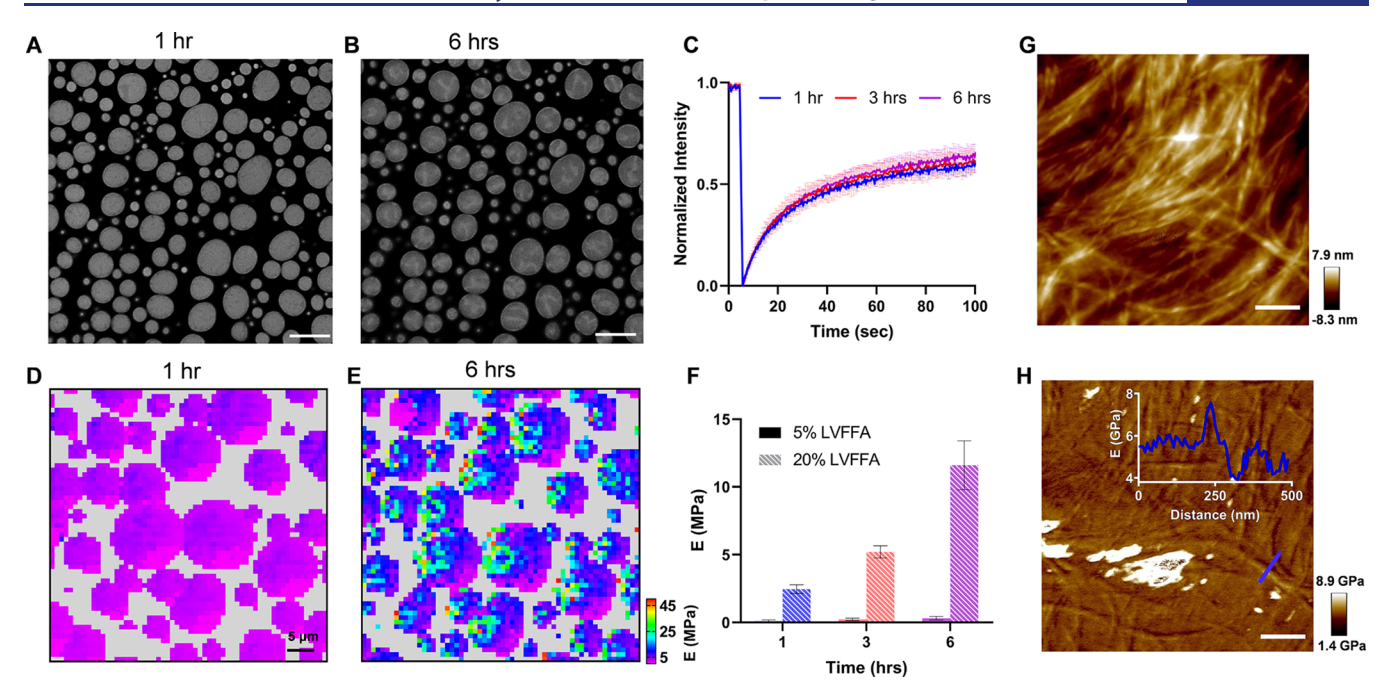


Figure 3. Dynamics of fiber growth inside condensates. (a, b) Confocal images of coacervates with 20% LVFFAR<sub>9</sub> over 1 and 6 h, respectively. Dye = 0.5% f-LVFFAR<sub>9</sub>, Scale bar =  $5 \mu$ m. (c) FRAP traces of coacervates over time formed with 20% LVFFAR<sub>9</sub>. Dye = 0.5% f-LVFFAR<sub>9</sub>. (d, e) Force maps showing Young's modulus (E in MPa) of coacervates with 20% LVFFAR<sub>9</sub> over 1 and 6 h, respectively. (f) Bar graph showing the average Young's modulus of condensates with various percentages of LVFFAR<sub>9</sub> over time. (g, h) Height and force maps, respectively, from AFM analysis of fibers formed by dried sample of 20% LVFFAR<sub>9</sub> condensates. Scale bar = 600 nm. Inset in (h) shows the variation of Young's modulus (E in GPa) over the topology marked in blue.

& S8) with no noticeable change in droplet size (Supporting Information Figure S12).

We hypothesized that the growth and maturation of amyloid fibers, inside condensates, should result in an increase in stiffness. To investigate this aspect, we performed solution-state AFM on the droplets over time (Figure 3d,e, Supporting Information Figure S13). The force maps show the distribution of Young's moduli (*E*) of these droplets over time, with average stiffness increasing from 2.5 to 12.5 MPa over 6 h, while nonamyloid containing droplets (5% LVFFAR<sub>o</sub>) only reach an average stiffness of 0.3 MPa (Figure 3f). The Young's modulus of LVFFAR<sub>9</sub> amyloid fibers formed in condensates (measured on dried samples of 20% LVFFAR<sub>9</sub> condensates) (Figure 3g,h, Supporting Information Figures S14 & S15) is in the range of 5— 8 GPa, which is orders of magnitude higher than the matured condensates. While it was not possible to directly measure Young's modulus of individual fibers inside droplets, this observation underscores how the droplets' mechanical stiffness is affected by the growth of fibers over time inside these droplets, while still retaining their liquid-like properties.

In conclusion, we show that a multicomponent assembly with designed components to generate amyloid-like fibers inside coacervates gives rise to local domains of ordered structures in liquid droplets. We further investigate these systems through a detailed microscopic analysis showing fibril maturation inside condensates. We note that peptide amphiphiles are known to form amyloid fibers in oil and water emulsions, where they have the tendency to accumulate at the interface. The key challenge that our design overcomes is that the amyloid assembly remains dispersed inside the liquid droplets, which opens up opportunities to study the properties and functions of supramolecular fibers inside liquid compartments. This is of significant consequence as a design feature for functional,

multicomponent condensates inside cellular environments that take advantage of their heterogeneity to drive a plethora of metabolic modifications. Additionally, this work lends insight into potential mechanisms for curbing uncontrolled amyloid growth associated with disease in living systems. We thus provide a first set of design principles to generate such systems synthetically.

#### ASSOCIATED CONTENT

#### **Supporting Information**

The Supporting Information is available free of charge at https://pubs.acs.org/doi/10.1021/jacs.2c05897.

Confocal image Z stacks of condensates formed with 20% LVFFAR<sub>9</sub>. Overlap channels of dyes *f*-LVFFAR<sub>9</sub> and *f*-ATP (MP4)

3D visualization of Z stacks presented in Video 1 processed by Imaris 9.7 (Oxford instruments, Zurich, Switzerland) (MP4)

FRAP of condensates formed with 20% LVFFAR<sub>9</sub>. Dye: 0.5% *f*-LVFFAR<sub>9</sub>. Video speed: 5× (AVI)

Fusion kinetics of pre-aged (2 hrs) of condensates formed with 20% LVFFAR<sub>9</sub>. Fusion event marked by white arrow. Dye: 0.5% *f*-LVFFAR<sub>9</sub>. Video speed: 4× (MP4) Aged (6 hrs) condensates formed with 20% LVFFAR<sub>9</sub> after addition of 3M NaCl. Dye: 0.5% *f*-LVFFAR<sub>9</sub>. Video speed: 6.3× (AVI)

Aged (6 hrs) condensates formed with 0% LVFFAR<sub>9</sub> after addition of 3M NaCl. Dye: 0.5% *f*-LVFFAR<sub>9</sub>. Video speed:  $7\times$  (AVI)

FRAP of aged (3 hrs) condensates formed with 20% LVFFAR<sub>9</sub> Dye: 0.5% *f*-LVFFAR<sub>9</sub>. Video speed: 5× (AVI) FRAP of aged (6 hrs) condensates formed with 20% LVFFAR<sub>9</sub> Dye: 0.5% *f*-LVFFAR<sub>9</sub>. Video speed: 5× (AVI)

Materials and methods, descriptions of Supporting Information Video files, confocal images, other images, plotted data (PDF)

#### AUTHOR INFORMATION

#### **Corresponding Authors**

Rein V. Ulijn — Nanoscience Initiative at Advanced Science Research Center, Graduate Center of the City University of New York, New York, New York 10031, United States; Ph.D. Programs in Biochemistry and Chemistry, The Graduate Center of the City University of New York, New York, New York 10016, United States; Department of Chemistry Hunter College, City University of New York, New York, New York 10065, United States; Orcid.org/0000-0002-7138-1213; Email: rulijn@gc.cuny.edu

Shana Elbaum-Garfinkle — Structural Biology Initiative at Advanced Science Research Center, Graduate Center of the City University of New York, New York, New York 10031, United States; Ph.D. Programs in Biochemistry and Chemistry, The Graduate Center of the City University of New York, New York, New York 10016, United States; Email: selbaumgarfinkle@gc.cuny.edu

Ankit Jain — Nanoscience Initiative at Advanced Science Research Center, Graduate Center of the City University of New York, New York, New York 10031, United States; Email: ajain@gc.cuny.edu

#### **Authors**

Salma Kassem — Nanoscience Initiative at Advanced Science Research Center, Graduate Center of the City University of New York, New York, New York 10031, United States

Rachel S. Fisher — Structural Biology Initiative at Advanced Science Research Center, Graduate Center of the City University of New York, New York, New York 10031, United States

Biran Wang — Molecular Cytology, Memorial Sloan Kettering Cancer Center, New York, New York 10065, United States; orcid.org/0000-0001-6637-6156

Tai-De Li — Nanoscience Initiative at Advanced Science Research Center, Graduate Center of the City University of New York, New York, New York 10031, United States; Department of Physics, City College of New York, City University of New York, New York, New York 10031, United States

Tong Wang – Nanoscience Initiative at Advanced Science Research Center, Graduate Center of the City University of New York, New York, New York 10031, United States

Ye He — Neuroscience Initiative at Advanced Science Research Center, Graduate Center of the City University of New York, New York, New York 10031, United States; Division of Science, The City College of New York, New York, New York 10031, United States

Complete contact information is available at: https://pubs.acs.org/10.1021/jacs.2c05897

#### **Author Contributions**

•Equal contribution.

#### **Notes**

The authors declare no competing financial interest.

#### ACKNOWLEDGMENTS

R.V.U. acknowledges funding from Office of Naval Research for the Vannevar Bush Faculty Fellowship (Grant No. N00014-21-1-2967). We thank the Air Force Office of Scientific Research for funding of R.V.U., S.E.G, A.J., R.F. (Grant No. FA9550-21-1-0091) and R.V.U. and S.K. (Grant No. FA9550-19-1-0111).

#### REFERENCES

- (1) Brangwynne, C. P.; Eckmann, C. R.; Courson, D. S.; Rybarska, A.; Hoege, C.; Gharakhani, J.; Jülicher, F.; Hyman, A. A. Germline P granules are liquid droplets that localize by controlled dissolution/condensation. *Science* **2009**, 324 (5935), 1729–32.
- (2) Astoricchio, E.; Alfano, C.; Rajendran, L.; Temussi, P. A.; Pastore, A. The Wide World of Coacervates: From the Sea to Neuro-degeneration. *Trends Biochem. Sci.* **2020**, *45* (8), 706–717.
- (3) Abbas, M.; Lipiński, W. P.; Wang, J.; Spruijt, E. Peptide-based coacervates as biomimetic protocells. *Chem. Soc. Rev.* **2021**, *50* (6), 3690–3705
- (4) Yewdall, N. A.; André, A. A. M.; Lu, T.; Spruijt, E. Coacervates as models of membraneless organelles. *Curr. Opin. Colloid Interface Sci.* **2021**, *52*, 101416.
- (5) Poudyal, R. R.; Guth-Metzler, R. M.; Veenis, A. J.; Frankel, E. A.; Keating, C. D.; Bevilacqua, P. C. Template-directed RNA polymerization and enhanced ribozyme catalysis inside membraneless compartments formed by coacervates. *Nat. Commun.* **2019**, *10* (1), 490.
- (6) Lu, T.; Spruijt, E. Multiphase Complex Coacervate Droplets. J. Am. Chem. Soc. 2020, 142 (6), 2905–2914.
- (7) Banani, S. F.; Lee, H. O.; Hyman, A. A.; Rosen, M. K. Biomolecular condensates: organizers of cellular biochemistry. *Nat. Rev. Mol. Cell Biol.* **2017**, *18* (5), 285–298.
- (8) Fisher, R. S.; Elbaum-Garfinkle, S. Tunable multiphase dynamics of arginine and lysine liquid condensates. *Nat. Commun.* **2020**, *11* (1), 4628
- (9) Mountain, G. A.; Keating, C. D. Formation of Multiphase Complex Coacervates and Partitioning of Biomolecules within them. *Biomacromolecules* **2020**, *21* (2), 630–640.
- (10) Mitrea, D. M.; Kriwacki, R. W. Phase separation in biology; functional organization of a higher order. *Cell Commun. Signal.* **2016**, *14* (1), 1.
- (11) Elbaum-Garfinkle, S.; Kim, Y.; Szczepaniak, K.; Chen, C. C.-H.; Eckmann, C. R.; Myong, S.; Brangwynne, C. P. The disordered P granule protein LAF-1 drives phase separation into droplets with tunable viscosity and dynamics. *Proc. Natl. Acad. Sci. U. S. A.* **2015**, *112* (23), 7189.
- (12) Ditlev, J. A.; Case, L. B.; Rosen, M. K. Who's In and Who's Out—Compositional Control of Biomolecular Condensates. *J. Mol. Biol.* **2018**, 430 (23), 4666–4684.
- (13) Chen, Y.; Yuan, M.; Zhang, Y.; Liu, S.; Yang, X.; Wang, K.; Liu, J. Construction of coacervate-in-coacervate multi-compartment protocells for spatial organization of enzymatic reactions. *Chemical Science* **2020**, *11* (32), 8617–8625.
- (14) Saha, B.; Chatterjee, A.; Reja, A.; Das, D. Condensates of short peptides and ATP for the temporal regulation of cytochrome c activity. *Chem. Commun.* **2019**, *55* (94), 14194–14197.
- (15) Klosin, A.; Oltsch, F.; Harmon, T.; Honigmann, A.; Jülicher, F.; Hyman, A. A.; Zechner, C. Phase separation provides a mechanism to reduce noise in cells. *Science* **2020**, *367* (6476), 464–468.
- (16) Deviri, D.; Safran, S. A. Physical theory of biological noise buffering by multicomponent phase separation. *Proc. Natl. Acad. Sci. U. S. A.* **2021**, *118* (25), e2100099118.
- (17) Fare, C. M.; Villani, A.; Drake, L. E.; Shorter, J. Higher-order organization of biomolecular condensates. *Open Biology* **2021**, *11* (6), 210137–210156.
- (18) Korkmazhan, E.; Tompa, P.; Dunn, A. R. The role of ordered cooperative assembly in biomolecular condensates. *Nat. Rev. Mol. Cell Biol.* **2021**, 22 (10), 647–648.
- (19) Patel, A.; Lee, H. O.; Jawerth, L.; Maharana, S.; Jahnel, M.; Hein, M. Y.; Stoynov, S.; Mahamid, J.; Saha, S.; Franzmann, T. M.;

- Pozniakovski, A.; Poser, I.; Maghelli, N.; Royer, L. A.; Weigert, M.; Myers, E. W.; Grill, S.; Drechsel, D.; Hyman, A. A.; Alberti, S. A Liquid-to-Solid Phase Transition of the ALS Protein FUS Accelerated by Disease Mutation. *Cell* **2015**, *162* (5), 1066–77.
- (20) Hsieh, M.-C.; Lynn, D. G.; Grover, M. A. Kinetic Model for Two-Step Nucleation of Peptide Assembly. *J. Phys. Chem. B* **2017**, *121* (31), 7401–7411.
- (21) Krishna Kumar, R.; Harniman, R. L.; Patil, A. J.; Mann, S. Self-transformation and structural reconfiguration in coacervate-based protocells. *Chemical Science* **2016**, *7* (9), 5879–5887.
- (22) McCall, P. M.; Srivastava, S.; Perry, S. L.; Kovar, D. R.; Gardel, M. L.; Tirrell, M. V. Partitioning and Enhanced Self-Assembly of Actin in Polypeptide Coacervates. *Biophys. J.* **2018**, *114* (7), 1636–1645.
- (23) Mohammadi, P.; Jonkergouw, C.; Beaune, G.; Engelhardt, P.; Kamada, A.; Timonen, J. V. I.; Knowles, T. P. J.; Penttila, M.; Linder, M. B. Controllable coacervation of recombinantly produced spider silk protein using kosmotropic salts. *J. Colloid Interface Sci.* **2020**, *560*, 149–160.
- (24) te Brinke, E.; Groen, J.; Herrmann, A.; Heus, H. A.; Rivas, G.; Spruijt, E.; Huck, W. T. S. Dissipative adaptation in driven self-assembly leading to self-dividing fibrils. *Nat. Nanotechnol.* **2018**, *13* (9), 849–855
- (25) Mason, A. F.; Buddingh', B. C.; Williams, D. S.; van Hest, J. C. M. Hierarchical Self-Assembly of a Copolymer-Stabilized Coacervate Protocell. *J. Am. Chem. Soc.* **2017**, *139* (48), 17309–17312.
- (26) Boekhoven, J.; Brizard, A. M.; Stuart, M. C. A.; Florusse, L.; Raffy, G.; Del Guerzo, A.; van Esch, J. H. Bio-inspired supramolecular materials by orthogonal self-assembly of hydrogelators and phospholipids. *Chemical Science* **2016**, *7* (9), 6021–6031.
- (27) Maeda, Y.; Makhlynets, O. V.; Matsui, H.; Korendovych, I. V. Design of Catalytic Peptides and Proteins Through Rational and Combinatorial Approaches. *Annu. Rev. Biomed. Eng.* **2016**, *18* (1), 311–328.
- (28) Esler, W. P.; Stimson, E. R.; Ghilardi, J. R.; Lu, Y.-A.; Felix, A. M.; Vinters, H. V.; Mantyh, P. W.; Lee, J. P.; Maggio, J. E. Point Substitution in the Central Hydrophobic Cluster of a Human  $\beta$ -Amyloid Congener Disrupts Peptide Folding and Abolishes Plaque Competence. *Biochemistry* **1996**, *35* (44), 13914–13921.
- (29) Liu, R.; McAllister, C.; Lyubchenko, Y.; Sierks, M. R. Residues 17–20 and 30–35 of beta-amyloid play critical roles in aggregation. *Journal of Neuroscience Research* **2004**, 75 (2), 162–171.
- (30) Lakdawala, A. S.; Morgan, D. M.; Liotta, D. C.; Lynn, D. G.; Snyder, J. P. Dynamics and Fluidity of Amyloid Fibrils: A Model of Fibrous Protein Aggregates. *J. Am. Chem. Soc.* **2002**, *124* (51), 15150–15151.
- (31) Omosun, T. O.; Hsieh, M. C.; Childers, W. S.; Das, D.; Mehta, A. K.; Anthony, N. R.; Pan, T.; Grover, M. A.; Berland, K. M.; Lynn, D. G. Catalytic diversity in self-propagating peptide assemblies. *Nat. Chem.* **2017**, *9* (8), 805–809.
- (32) Sarkhel, B.; Chatterjee, A.; Das, D. Covalent Catalysis by Cross  $\beta$  Amyloid Nanotubes. *J. Am. Chem. Soc.* **2020**, 142 (9), 4098–4103.
- (33) Booth, R.; Insua, I.; Ahmed, S.; Rioboo, A.; Montenegro, J. Supramolecular fibrillation of peptide amphiphiles induces environmental responses in aqueous droplets. *Nat. Commun.* **2021**, *12* (1), 6421.
- (34) Scott, G. G.; McKnight, P. J.; Tuttle, T.; Ulijn, R. V. Tripeptide Emulsifiers. *Adv. Mater.* **2016**, 28 (7), 1381–1386.

### **□** Recommended by ACS

#### Molecular Architecture and Helicity of Bacterial Amyloid Nanofibers: Implications for the Design of Nanoscale Antibiotics

Paolo Elvati, Angela Violi, et al.

APRIL 19, 2023

ACS APPLIED NANO MATERIALS

READ 🗹

#### Molecular Modeling of Self-Assembling Peptides

Stephen J. Jones and Alberto Perez

FEBRUARY 16, 2023

ACS APPLIED BIO MATERIALS

READ 🗹

#### Supramolecular Assembly and Small-Molecule Binding by Protein-Engineered Coiled-Coil Fibers

Dustin Britton, Jin Kim Montclare, et al

OCTOBER 13, 2022

BIOMACROMOLECULES

READ 🗹

## Hollow Octadecameric Self-Assembly of Collagen-like Peptides

Le Tracy Yu, Jeffrey D. Hartgerink, et al.

FEBRUARY 22, 2023

JOURNAL OF THE AMERICAN CHEMICAL SOCIETY

READ 🗹

Get More Suggestions >